Experimental verification of active oscillation controller for vehicle drivetrain with backlash nonlinearity based on norm-limited SPSA

Heisei Yonezawa[#1], Ansei Yonezawa[#2], Itsuro Kajiwara [#3]

#1(Corresponding author)
Division of Mechanical and Aerospace Engineering, Hokkaido University
N13, W8, Kita-ku, Sapporo 060-8628, Japan
Phone +81-80-4039-9406
E-mail: yonezawah@eng.hokudai.ac.jp

#2
Division of Mechanical and Aerospace Engineering, Hokkaido University
N13, W8, Kita-ku, Sapporo 060-8628, Japan
Phone +81- 90-2893-3160
E-mail: ayonezawa@eng.hokudai.ac.jp

#3
Division of Mechanical and Aerospace Engineering, Hokkaido University
N13, W8, Kita-ku, Sapporo 060-8628, Japan
Phone +81-11-706-6390, Fax. +81-11-706-6390
E-mail: ikajiwara@eng.hokudai.ac.jp

Abstract

To address vehicle drivetrain vibrations that cause discomfort and poor drivability, this study proposes a new active damping strategy with simple backlash compensation based on the simultaneous perturbation stochastic approximation (SPSA) with norm-limited update vector. First, an experimental device developed for a simplified drivetrain mechanism is demonstrated. A mechanism for reproducing both the contact mode and the backlash mode is included in the device. For the contact mode, a model-based H_2 controller is employed as the baseline damping strategy. Further, to mitigate the backlash effect, a simple algorithm based on mode-switching-based compensation is used with the H_2 controller. In particular, for the critical controller parameters, this paper presents a systematic design approach to search for their optimal values. The key parameters, which are needed for the backlash and contact mode controllers, are simultaneously auto-tuned using norm-limited update vector-based SPSA, which ensures the stability in the iterative tuning. The novelty of this study is that both the backlash mode controller and the contact mode controller are simultaneously optimized by the improved version of SPSA, thus realizing a comprehensive auto-tuning design of an active drivetrain damping system. Finally, the active controller is experimentally verified using the actual test device. Comparative studies show that the proposed approach significantly reduces drivetrain vibrations and is robust against fluctuations in the backlash.

Keywords: Powertrain, Active vibration control, Drivetrain, Backlash, Optimization, Simultaneous perturbation stochastic approximation, Vibration, Vehicle system

1. Introduction

Vibrations cause noise, fatigue failure, and discomfort, providing an adverse influence for mechanical systems. The need for vibration suppression technology has grown as a result of the current movement toward downsizing, greater comfort, weight reduction, and superior performance.[1,2,3] Due to their potential to deliver strong dampening effects for intricate mechanical systems, active vibration damping has received a lot of research attention.

Vehicle drivetrains also require vibration control as one of the essential important technologies to maintain their functions. Vibrations induced by a sudden driving force change in the drivetrain[4] of a vehicle persist as a serious problem. These vibrations not only degrade the comfort and drivability but also reduce the durability of the drivetrain components. As one of the promising countermeasures, coupling a nonlinear dynamic vibration absorber in parallel to a drivetrain mechanism can be considered. For example, a nonlinear energy sink (NES)[5,6] can efficiently dissipate vibrational energy through

structural damping by redistributing the vibration energy within the modal space of the primary structure or passively absorb a part of this energy from the drivetrain in a nearly irreversible form. The advantage is that it can operate over a broad range of frequencies. In the successful application to attenuation of drivetrain vibrations,[5] three types of NESs were investigated: a third-order NES stiffness, a vibro-impact non-smooth NES and a NES with fifth-order smooth nonlinear stiffness.

The use of NESs is categorized as passive vibration control, whereas this study focuses on developing the active vibration control method for drivetrain vibrations. NES is a lightweight absorber effective over a broad range of frequencies; however, active vibration control is also needed in order to obtain higher vibration suppression performances without increasing the weight of the driveline at all. Compared to passive control such as NESs, active control can provide stronger damping effects based on control algorithms by using only an existing actuator and does not need to incorporate additional palliative devices, thus reducing the associated costs. For the active vibration

control of the vehicle drivetrain, some advanced control strategies have been presented, such as compensation for a disturbance based on an adaptive observer[7] for damping control of internal combustion engine powered powertrains. Further, an adaptive active control scheme has been developed by combining model prediction and Butterworth filter control to solve the torsional vibration problem.[8] In addition, the filtered-x least mean square algorithm[9] and a model reference controller have been implemented.[10] Moreover, a previous work has improved vehicle drivability by using a linear quadratic tracking controller with a model reference adaptive technique.[11]

However, the aforementioned studies have not considered the nonlinear backlash existing in the gears of drivetrains. Backlash in a drivetrain leads to an undesirable phenomenon, which significantly increases the vibration amplitude.[12,13] The drivetrain dynamics switch between two conditions: “contact mode”, during which mechanical contact occurs, and “backlash mode”. Backlash mode disconnects the output side (wheel side) from the input side (actuator side) owing to the traversal in backlash. This

phenomenon, i.e., switching of the dynamics modes, also leads to higher complexity of control system structures and increases the designer's burden in terms of tuning tasks.

For a drivetrain with backlash, a hybrid strategy of a feedforward-feedback controller and a robust disturbance observer has been introduced to compensate for the backlash.[14] Sliding mode control-based approaches have also been investigated for a drivetrain with nonlinearity.[15,16] Another study has adopted a combination of linear quadratic regulator (LQR) and a notch filter for the contact mode while dealing with the backlash mode using a proportional integral differential (PID) controller.[17]

However, in the existing studies, the following shortcomings and rooms for improvement remain as:

- With respect to controller parameters that must be determined by designers, there has been no attempt to adopt efficient optimization for auto-tuning of the parameters.

- The mechanism of compensation for backlash can be improved by making it simpler with a lower online computational load. Moreover, versatility is desired to facilitate its use with a wide variety of model-based linear controllers for satisfactory vibration reduction in the contact mode.

The optimization design is closely related to the complicated powertrain dynamics.[18,19] Some researchers have employed efficient optimization algorithms for their applications, such as a gear shifting fuzzy controller and an engine management approach optimized using an advanced genetic algorithm with interactive adaptive-weight,[20,21] multi-objective optimization,[18] lookup-table-based torque control,[22] and design of a torsional vibration damper (a dual mass flywheel with an internal damper).[23] The aforementioned works suggest the following important aspects: (1) effectiveness of iterative offline simulations based on powertrain dynamics models; (2) necessity of application of efficient optimization algorithms (rather than the designer's subjective selection) to automatically search for the controller parameters.[19]

Focusing on active vibration controls of a drivetrain, their controller design can be framed as optimization problems. For the backlash mode, a previous study has developed a new clunk controller with model-based torque shaping.[12] It consists of a soft-landing reference governor and a proportional-derivative (PD) baseline controller to track the modified reference. The ingenious point is that the competing design requirements, i.e., reducing the clunk when the backlash traversal finishes and allowing the backlash to be crossed rapidly, are defined as an optimal control problem. However, a contact mode controller[12,24] and the aforementioned PD gains have not been included in auto-tuning optimization, although they are critical for addressing transient oscillations in a drivetrain. In addition, the optimization solution can be obtained more conveniently by introducing an efficient optimization algorithm. For the minimization of an objective function based on the root mean square (RMS) of drivetrain vibration responses, the LQR controller has been optimized offline.[25] The selection of the critical weighting matrices has been optimized with the genetic algorithm (GA). However, this

work does not consider the backlash nonlinearity in a drivetrain. Another study has proposed a safe calibration framework based on Bayesian optimization to obtain the optimal controller gain.[26] However, the backlash has not been explicitly addressed in the controller. Among previous approaches, the most popular choice for powertrain dynamics control is model predictive control (MPC).[27] To address undesired oscillations due to backlash, the online MPC, which is a quadratic form-defined optimal control in a receding horizon, has been implemented.[28] In the literatures,[29,30] switching strategies for multiple predictive controllers have addressed the nonlinearity in a powertrain. The MPC controller can produce ideal responses including little error states such as excessive jerks and transient oscillations.[31] Although MPC has achieved promising results, one of its main drawbacks is its high computational burden online. This makes it difficult to implement MPC on real-time applications without sacrificing the control performance.[12] Furthermore, the need to implement many different controllers makes the control structure more complicated, involving high requirements for the control module memory.

In summary, previous studies have not applied an optimization process for the contact mode controller or the backlash mode controller, i.e., auto-tuning of the controller parameters is insufficient. In addition, few studies have focused on developing a simple and versatile backlash compensation strategy with lower online computational loads. Therefore, the novelty and principal contributions of our work are to bridge these gaps.

Based on our previous works,[13,32] this study proposes an improved version of active drivetrain vibration control with compensation for backlash. In this paper, the active controller is verified using an actual test device of a simplified drivetrain mechanism with backlash. We employ the reduced drivetrain configuration similar to the existing work[5]: this is a reduced lumped parameter model composed of a few inertias connected via stiffness. The model in the work[5] incorporates all the nonlinearities in the equation of motion such as the nonlinear stiffness of NESs, the aerodynamic drag torque and the tire rolling resistance, whereas this study only considers the dead zone property due to

the backlash nonlinearity. This is because we need to focus on the effect of backlash and make it easier to evaluate the efficacy of the proposed backlash compensation. For considering the backlash and contact modes, the proposed control system is constructed as a simple compensation algorithm based on switching of the control modes, which can be applicable for a single model-based vibration controller. It can reduce the shock when a drivetrain is changed from the backlash mode to the contact mode while allowing the backlash to be traversed rapidly. Even though its versatility has been proven through some application examples with various model-based linear controllers,[13,32] its critical controller parameters require manual setting based on trial-and-error tuning by the designer.[32] In other words, an auto-tuning design based on an optimization algorithm needs to be newly introduced. The contributions of this paper can be summarized as follows.

1) As a novelty of this study compared to previous studies, both the backlash mode controller (i.e., a soft-landing compensator) and the contact mode controller (i.e., a

baseline H_2 vibration suppression) are simultaneously optimized, resulting in the realization of an auto-tuning design. This auto-tuning optimization reduces the designer's burden as well as the cost of trial-and-error procedures.

2) As a tuning algorithm, the simultaneous perturbation stochastic approximation with a norm-limited update vector (hereafter referred to as "NLSPSA" in this paper) is employed. This work is the first to propose the application of NLSPSA for active damping of a drivetrain. This enables a high calculation efficiency while guaranteeing the stability of the iterative tuning process.

3) To realize compensation for backlash, a simpler algorithm based on switching of the control modes is combined with a single output feedback H_2 controller. Its advantages include not only lower online computational requirements, but also reduction in complexity of the control structure.

4) Compared to a previous study that has only performed simulation tests,[33] this study experimentally confirms the effectiveness of the proposed method using an actual test device of a simplified drivetrain mechanism with backlash.

2. Basic experimental device

2.1. Simplified drivetrain with backlash

As the controlled object, this study considers a basic experimental device. By simplifying the actual driveline mechanism, this allows us to concentrate on the oscillation phenomena brought on by backlash effects and an abrupt shift in driving force. The device specifications are summarized in Table 1. The mechanical model and the actual test rig are given in Figs. 1(a) and (b), respectively. The structure is a three-degree-of-freedom translational vibration system that is equivalent to a simplified drivetrain.[13,34] The three mass points (M_E, m_G, M_B) are connected via springs and dampers. Backlash is produced as a dead-zone band by providing a large adjustable

space between the plate springs on both sides of m_G. Further details on the experimental device, such as the simplifications, can be found in Refs.[13,35] The motor acts as the actuator to realize the control input.

Figs. 1(c) and (d) show the contact mode and the backlash mode, respectively. In the contact mode, the mechanical connection is established between the actuator and the vehicle body side. By contrast, the backlash mode is a disconnected situation during the backlash traversal.

Table 1 Specifications of the test device

Parameter	Value	Unit
K_D	2.2×10^4	N/m
K_C	660.0	N/m
K_G	5.3×10^4	N/m
m_G	0.039	kg
M_B	0.232	kg
M_E	1.04	kg
C_C	0.1	Ns/m
C_{cl}	1.5	Ns/m
C_G	36.0	Ns/m
C_D	12.5	Ns/m

2.2. State-space representation for modeling

For the purpose of deriving a baseline vibration controller used in the contact mode, we need a linearized plant model because the experimental device involves nonlinearities such backlash. As indicated below, the previous works have already derived the linear state-space representation of the plant dynamics in the form of the time-varying state equation.[13,35]

$$\dot{\boldsymbol{x}}_p = \boldsymbol{A}_p \boldsymbol{x}_p + \boldsymbol{B}_{p1} \boldsymbol{w}_p + \boldsymbol{B}_{p2} u \tag{1}$$

$$y_p = \boldsymbol{C}_p \boldsymbol{x}_p + \boldsymbol{D}_{p1} \boldsymbol{w}_p + D_{p2} u \tag{2}$$

Each coefficient matrix and the state vector are expressed as follows:

$$\boldsymbol{A}_p = \begin{bmatrix} 0 & 0 & 0 & 1 & 0 & 0 \\ 0 & 0 & 0 & 0 & 1 & 0 \\ 0 & 0 & 0 & 0 & 0 & 1 \\ -\frac{(K_D + K_C)}{M_B} & \frac{K_D}{M_B} & 0 & -\frac{(C_D + C_C)}{M_B} & \frac{C_D}{M_B} & 0 \\ \frac{K_D}{m_G} & -\frac{(SwK_G + K_D)}{m_G} & \frac{SwK_G}{m_G} & \frac{C_D}{m_G} & -\frac{(SwC_G + C_D)}{m_G} & \frac{SwC_G}{m_G} \\ 0 & \frac{SwK_G}{M_E} & -\frac{SwK_G}{M_E} & 0 & \frac{SwC_G}{M_E} & -\frac{(SwC_G + C_{cl})}{M_E} \end{bmatrix}$$

$$\boldsymbol{B}_{p1} = \begin{bmatrix} 0 & 0 \\ 0 & 0 \\ 0 & 0 \\ 0 & \frac{1}{M_B} \\ \frac{1}{m_G} & 0 \\ -\frac{1}{M_E} & 0 \end{bmatrix}, \quad \boldsymbol{B}_{p2} = \begin{bmatrix} 0 \\ 0 \\ 0 \\ 0 \\ 0 \\ \frac{1}{M_E} \end{bmatrix}, \quad \boldsymbol{C}_p = [\,1 \quad 0 \quad 0 \quad 0 \quad 0 \quad 0\,] \tag{3}$$

$$\boldsymbol{D}_{p1} = 0, \quad D_{p2} = 0$$

$$\boldsymbol{x}_p = [X_B \quad x_G \quad X_E \quad \dot{X}_B \quad \dot{x}_G \quad \dot{X}_E]^T \tag{4}$$

In Eqs. (1) and (2), u is the control input and $\boldsymbol{w}_p$ is the disturbance including the force due to the backlash. By switching the parameter Sw, the dead-zone characteristic of the backlash can be expressed. The switching rule is shown below.[36,37] Here, a force, which originates from the spring K_G, is denoted as F. The width of a dead zone by the backlash effect is denoted as $|bl|$. Sw is set to 1.0 in design of the baseline controller.

$$\begin{aligned} &F = OKG + Sw \cdot K_G \cdot \Delta X, \quad \Delta X = X_E - x_G \\ &Sw = \begin{cases} 1, & \Delta X > |bl| \\ 1, & \Delta X < -|bl| \\ 0, & |\Delta X| \le |bl| \end{cases} \\ &OKG = \begin{cases} 0, & |\Delta X| \le |bl| \\ -|K_G \times |\delta||, & \Delta X > |bl| \\ |K_G \times |\delta||, & \Delta X < -|bl| \end{cases} \end{aligned} \tag{5}$$

The experimental device, which involves nonlinear characteristics such as backlash, has been modeled by the time-varying linear state equation, which is more detailed in the previous study.[13]

3. Active vibration control with compensation for backlash

The entire control structure consists of two main parts: the contact mode control (baseline vibration suppression) and the backlash mode control (simple mode-switching-based compensation). The control structure is shown in Fig. 2.

3.1. Model-based H_2 vibration controller

As the baseline controller, a model-based linear H_2 controller is designed to achieve high damping effects and excellent transient responses.[38,39]

Fig. 3 shows the block diagram used to design the H_2 baseline controller. Here, z_y and z_u denote the controlled variables with respect to transient response of the oscillation of the vehicle body and penalty on the amount of the control input (energy saving), respectively. The vehicle vibration y indicates the observed output. u and w denote the control input and disturbance containing the force owing to the effect of backlash, respectively. P_c, $F_{Highpass}$, and $F_{Lowpass}$ denote the controlled object including an integrator, a high-pass filter, and a frequency transfer function of a

low-pass filter including a first-order lag element, respectively.[13,32] The expanded controlled object $G(s)$ is constructed to eliminate unmodeled uncertain dynamics in a high-frequency band.[13] As discussed later, Q_k and R_k are weighting constants, i.e., critical tuning parameters, for the controller design. k is the number of iterations for the optimization, which is explained later.

From the external input to $z = [z_y \quad z_u]^T$, a transfer function $T_{zw}(s)$ can be defined. Therefore, the baseline vibration controller is designed such that the H_2 norm $\|T_{zw}(s)\|_2^2$ is minimized.[38] The design approach is implemented utilizing the Robust Control Toolbox and Control System Toolbox, which are installed n MATLAB.

When evaluating the H_2-norm criterion, z_u and z_y are defined as the multiplication of the control input u_G and the vehicle vibration y_G from the expanded controlled object by the evaluation weights $\sqrt{R_k}$ and $\sqrt{Q_k}$, respectively, as follows:

$$z_y = \sqrt{Q_k} \cdot y_G \tag{6}$$

$$z_u = \sqrt{R_k} \cdot u_G \tag{7}$$

Equations (6) and (7) imply that Q_k and R_k are the critical parameters affecting the vibration attenuation performance. Because they amplify y_G and u_G via the multiplication, how much to highlight each of the vibration response and the control input limitation is directly determined in the H_2-norm minimization. Consequently, trial-and-error adjustments for effective balancing between Q_k and R_k have been imposed in our previous studies.[32]

3.2. Backlash compensation by simple control mode switching algorithm

During the backlash mode, the aims of our backlash compensation strategy are as follows:

- to push the backlash to travel from negative contact towards positive contact as soon as possible for good responsiveness;
- to reduce the impact (shock) when the drivetrain is transferred from the backlash mode to the contact mode and the backlash traversal finishes by soft landing.

To meet these competing requirements, the compensation algorithm based on switching of the control modes is applied to the baseline H_2 vibration controller.[13,16] This is outlined in Fig. 4. The backlash can be traversed quickly yet smoothly with the help of this compensation, which also eliminates the accumulation (buildup) of control errors in the backlash.

In Eqs. (8)-(10) and Fig. 4, as the contact mode controller that operates during the mechanical contact, the normal H_2 vibration control is performed. The low-frequency resonance should be attenuated during the contact mode.

In Eqs. (11)-(15), the compensation during the backlash traversal is performed by the backlash mode controller. Here, by switching the target signal $r(n)$ to a small positive value r_k^{BL} that is a key compensation reference signal (parameter) for realizing soft landing, the backlash can be traversed gently and rapidly. This is because the control error $e_{BL}(n)$ originating from r_k^{BL} makes the H_2 controller compute the moderate

input command for the backlash traversal. The dead-zone effect due to the backlash causes excessive control errors to accumulate in the controller, resulting in a shock with the calculation of a large control command. Therefore, anti-windup needs to be introduced. Specifically, for the discretized controller $(\boldsymbol{A}_{ck}, \boldsymbol{B}_{ck}, \boldsymbol{C}_{ck}, D_{ck})$, the updating of the state vector $\boldsymbol{x}_c(n)$ is temporarily stopped by anti-windup. This processing avoids the undesired effect caused by the dead-zone in the backlash, i.e., the cumulation (buildup) of the control errors. The controller with a frozen state vector no longer unnecessarily accelerates the actuator during the backlash traversal.

Due to this compensation, we can prevent unnecessary excessive control inputs during the backlash traversal, resulting in a considerably reduced shock with a collision in the backlash. Refer the previous studies[13,32] for further details on the basic idea of this compensation.

Note that the same single H_2 controller is commonly used in both the backlash mode and the contact mode. Its discretized state space representation is shown as $(\boldsymbol{A}_{ck}, \boldsymbol{B}_{ck}, \boldsymbol{C}_{ck}, D_{ck})$. This simple mechanism means that multiple controllers according to the mode switching do not need to be prepared.

(Contact mode control):

$$\boldsymbol{x}_c(n+1) = \boldsymbol{A}_{ck}\boldsymbol{x}_c(n) + \boldsymbol{B}_{ck}e(n) \quad (8)$$

$$u_{CO}(n) = \boldsymbol{C}_{ck}\boldsymbol{x}_c(n) + D_{ck}e(n) + K_C r(n) \quad (9)$$

$$e(n) = r(n) - X_B(n) \quad (10)$$

(Backlash mode control):

$$\boldsymbol{x}_{AW}(n+1) = \boldsymbol{A}_{ck}\boldsymbol{x}_c(n) + \boldsymbol{B}_{ck}e_{BL}(n) \quad (11)$$

$$\boldsymbol{x}_{AW}(n) = z^{-1}[\boldsymbol{x}_{AW}(n+1)] \quad (\boldsymbol{x}_{AW}(n) = \boldsymbol{x}_c(n)) \quad (12)$$

$$\boldsymbol{x}_c(n+1) = \boldsymbol{x}_{AW}(n) \quad \text{i.e., Substitute } \boldsymbol{x}_{AW}(n) \text{ for } \boldsymbol{x}_c(n+1) \quad (13)$$

$$u_{BL}(n) = \boldsymbol{C}_{ck}\boldsymbol{x}_c(n) + D_{ck}e_{BL}(n) + K_C r_k^{BL} \quad (14)$$

$$e_{BL}(n) = r_k^{BL}(n) - X_B(n) = r_k^{BL} - X_B(n) \quad (15)$$

To identify the moment at which the drivetrain is transferred from the backlash mode to the contact mode and the backlash traversal finishes, a vehicle jerk can be utilized. The vehicle body acceleration with regard to time is differentiated to produce a jerk. Specifically, we need a threshold condition as follows:

$$|Jerk(n)| \geq Threshold \quad (16)$$

With discontinuous change of the vehicle acceleration owing to the mode switching, the steep jerk value is well suited for the judgement because it can be observed independently of the backlash length fluctuation. Moreover, the use of the vehicle body jerk contributes to simplification of the compensation structure.

The soft-landing reference r_k^{BL} during the backlash mode significantly affects the vibration control performance. If this value is too large, unsuccessful soft landing will cause an impact (shock) because an excessive control input command will be given to the actuator. Meanwhile, if r_k^{BL} is too small, the responsiveness will be poor. Achieving an effective balance is a challenging task, and it has been manually tuned with trial-and-error adjustments in our previous studies.[13,32]

4. Auto-optimization scheme for the backlash and contact mode controllers

4.1. SPSA with norm-limited update vector

The proposed tuning approach employs SPSA because of its calculation efficiency. The algorithm of SPSA updates a design variable $\theta \in \mathbb{R}^p$ so that a non-negative scalar loss function $L(\theta)$ is minimized. At the kth iteration, the update rule is given as shown in Eq. (17).[40] The gradient $g(\theta) = \partial L/\partial\theta = \nabla L(\theta)$ is stochastically estimated. The estimated gradient is denoted as $\hat{g}_k(\theta_k) \in \mathbb{R}^p$ in the kth iteration. The ith element of $\hat{g}_k$ is $\hat{g}_{k,i}$. $\Delta_k \in \mathbb{R}^p$ is a random perturbation vector, which contains each component $\Delta_{k,i}$. A typical selection of $\Delta_k \in \mathbb{R}^p$ is Bernoulli distribution, which generates ± 1.[41] For all k, i, $\Delta_{k,i}$ with finite inverse moments $E[|\Delta_{k,i}{}^{-1}|]$ should be symmetrically distributed about 0 and independent.[40,42]

$$\theta_{k+1} = \theta_k - a_k \hat{g}_k(\theta_k) \tag{17}$$

$$\hat{g}_{k,i}(\theta_k) = \frac{L(\theta_k + c_k\Delta_k) - L(\theta_k - c_k\Delta_k)}{2c_k\Delta_{k,i}} \tag{18}$$

$$\Delta_k = [\Delta_{k,1} \quad \Delta_{k,2} \quad \cdots \quad \Delta_{k,p}]^T \tag{19}$$

Equations (20)-(23) are the conditions to be satisfied in selections of the gain sequences a_k and c_k.[40] With positive constants a, A, c, α, and γ, a_k and c_k are typically set, as indicated in Eqs. (24) and (25).[40,42]

$$a_k > 0, c_k > 0 \tag{20}$$

$$\lim_{k\to\infty} a_k \to 0, \lim_{k\to\infty} c_k \to 0 \tag{21}$$

$$\sum_{k=1}^{\infty} a_k = \infty \tag{22}$$

$$\sum_{k=1}^{\infty} \frac{{a_k}^2}{{c_k}^2} < \infty \tag{23}$$

$$a_k = \frac{a}{(A+k)^{\alpha}} \tag{24}$$

$$c_k = \frac{c}{k^{\gamma}} \tag{25}$$

High calculating efficiency is one of SPSA's benefits. According to equation (18), $\hat{g}_k$ can be estimated using just two L computations (i.e., two loss function measurements), and it is not reliant on the design variable θ_k's size p.[40] Calculating the loss function value is typically the most challenging work (time and cost consuming step) in many engineering optimizations.[43,44] Hence, especially in multi-dimensional optimizations, SPSA is highly efficient because few loss function computations are needed at each iteration. This benefit has resulted in practical controller tuning applications.[44]

However, several researchers have indicated that the computation stability should be improved to apply SPSA for practical applications.[45] An effective approach is to

explicitly limit the updating amount of design variable.[45] Therefore, the term $a_k\hat{g}_k(\theta_k)$ is saturated as follows:

$$\theta_{k+1} = \theta_k - \delta(a_k\hat{g}_k(\theta_k)) \tag{26}$$

$$\delta\left(a_k\hat{g}_k(\theta_k)\right) = \begin{bmatrix} \mathrm{sgn}\left(a_k\hat{g}_{k,1}\right)\min\left\{\left|a_k\hat{g}_{k,1}\right|, d\right\} \\ \mathrm{sgn}\left(a_k\hat{g}_{k,2}\right)\min\left\{\left|a_k\hat{g}_{k,2}\right|, d\right\} \\ \vdots \\ \mathrm{sgn}\left(a_k\hat{g}_{k,p}\right)\min\left\{\left|a_k\hat{g}_{k,p}\right|, d\right\} \end{bmatrix} \tag{27}$$

In addition, by restricting $\Delta_k \in \mathbb{R}^p$ to a Bernoulli distribution, Eq. (27) can be simply rewritten as follows:

$$\delta\left(a_k\hat{g}_k(\theta_k)\right) = \min\left\{\left|\frac{a_k\Delta L}{2c_k}\right|, d\right\}\begin{bmatrix} \mathrm{sgn}\left(\Delta L/\Delta_{k,1}\right) \\ \mathrm{sgn}\left(\Delta L/\Delta_{k,2}\right) \\ \vdots \\ \mathrm{sgn}\left(\Delta L/\Delta_{k,p}\right) \end{bmatrix} \tag{28}$$

$$\Delta L = L(\theta_k + c_k\Delta_k) - L(\theta_k - c_k\Delta_k) \tag{29}$$

This improved version is referred to as SPSA with a norm-limited update vector (NLSPSA). Here, $\delta: \mathbb{R}^p \to \mathbb{R}^p$ in Eq. (26) shows the saturation function, where $d > 0$ denotes the scalar-valued constant. The remarkable point of this modified algorithm is that a theoretical analysis of the convergence of Eq. (26) has been provided.[45] Note that each element of $\delta\left(a_k\hat{g}_k(\theta_k)\right)$ is limited within $[-d,\ d]$; thus, the instability of the iterative optimization process is avoided. This paper is the first to demonstrate the

application of NLSPSA for controlling a drivetrain with backlash, to the best of our knowledge.

4.2. Norm-limited SPSA-based parameter tuning scheme

For the backlash mode and the contact mode, a parameter tuning scheme is newly proposed on the basis of NLSPSA. The tuning scheme is given in Fig. 5. In the following, "design variables ($\theta_k \in \mathbb{R}^p$)" refers to the parameters that NLSPSA directly updates in Eq. (26). "Tuning parameters" refers to the parameters that designers must determine to derive a controller. For evaluating the active damping performance, we need to set a loss function $J(\theta_k)$, which takes non-negative values. In Fig. 5, NLSPSA searches for the θ_k that minimizes $J(\theta_k)$. $C_{stop} \in \mathbb{N}$ indicates a stop criterion, i.e., the total number of iterations.

An advantage of the proposed method is that both the contact mode controller (i.e., the H_2 baseline controller) and the backlash mode controller (i.e., the soft-landing

compensator) can be simultaneously and automatically optimized. The proposed approach can reduce not only the subjective selection of the critical controller parameters by the designer, but also the load on the designer caused by laborious trial-and-error processes.

4.3. Tuning parameter expression

The proposed method automatically tunes all of Q_k, R_k, and r_k^{BL} in Eqs. (6), (7), and (15), resulting in the simultaneous optimization for the compensator in the backlash mode and the H_2 controller in the contact mode. That is, the tuning parameters are Q_k, R_k, and r_k^{BL} in this research. Equations (30)-(32) express Q_k, R_k, and r_k^{BL} using the design variable θ_k.

$$Q_k = |\theta_{k,1}|Q_0 \tag{30}$$

$$R_k = |\theta_{k,2}|R_0 \tag{31}$$

$$r_k^{BL} = |\theta_{k,3}|r_0^{BL} \tag{32}$$

$\theta_{k,i}$ represents the ith component of θ_k. Q_0 is the initial value of Q_k, and R_0 is that of R_k. Similarly, r_0^{BL} is the initial value of r_k^{BL}. Therefore, θ_k is a three-dimensional variable. For the backlash and contact modes, all the critical design variables are stored

in θ_k. The initial values of those are set as $Q_0 = 1.0$, $R_0 = 1.0$, and $r_0^{BL} = 1.0 \times 10^{-1}$ in this research.

4.4. Loss function in optimization

The proposed tuning design uses the loss function $J(\theta_k)$ shown in Eq. (33).

$$J(\theta_k) = J_k = \frac{1}{N}\left\{W_y\left(\sum_{n=1}^{N} {\tilde{y}_{k,n}}^2\right) + W_u\left(\sum_{n=1}^{N} {u_{k,n}}^2\right)\right\} \quad (33)$$

Here, $\tilde{y}_{k,n}$ is the control error between an ideal target response and the vibration response (observed output) at the kth iteration at the nth sampling step. $u_{k,n}$ indicates the control input component for vibration suppression at the kth iteration at the nth sampling step. In each simulation, the number of sampling points is denoted as N. The scaling factors on $\tilde{y}_{k,n}$ and $u_{k,n}$ are W_y and W_u, respectively. By taking into account the scale gap between the two terms in Eq. (33), they are set to $W_y = 10^3$ and $W_u = 1$. $J(\theta_k)$ is therefore defined as the mean square of $\tilde{y}_{k,n}$ plus that of $u_{k,n}$ derived from the vibration suppression controller with θ_k.

4.5. Parameter tuning condition

Table 2 lists the conditions for NLSPSA shown in Eqs. (17)–(29). They are determined according to the guideline on SPSA implementation.[41] The simulation time in each iteration is 4.0 s.

Table 2. Conditions for NLSPSA in the proposed method.

Properties	Value
Number of iterations	100
α	0.602
θ_0	$[1 \quad 1 \quad 1]^T$
c	1.0×10^{-1}
a	7.0×10^{-4}
A	1.0×10^{0}
d	40
γ	0.101
Δ_k	Bernoulli distribution with probability of 1/2 for each ± 1

4.6. Tuning results

Here, the tuning results obtained by the proposed method are discussed. Figures 6 and 7 show the tuning histories of each tuning parameter and the value of $J(\theta_k)$ by iteration,

respectively. Note that Fig. 6(c) shows that r_k^{BL} converges to a small non-zero positive value.

Fig. 7 means that the auto-tuned (resultant) controller suppresses vibrations sufficiently. The successful tuning history is observed in Fig. 7, where the initial large value of $J(\theta_k)$ eventually converges to a small positive value. Table 3 summarizes the tuning results shown in Figs. 6 and 7. These results quantitatively reflect the improvement of the control performance by iteration.

Table 3. Tuning result of the CO and BL controller parameters (mean of 5 trials).

Properties	Value
Q_{100}	20.9217
R_{100}	31.4235
r_{100}^{BL}	0.008371397
J_0	2.0134×10^4
J_{100}	4.197

5. Experimental verifications

5.1. Setting of experimental verifications

In this study, the active damping system is implemented on the experimental system, and the effectiveness is validated using the actual test device. Figure 8 shows the closed-loop diagram of the experimental verifications. The aim of the controllers is to damp the vehicle vibration X_B and thus realize an ideal target response. The vehicle body vibration is measured with a laser sensor (KEYENCE, IL-300). The measured signal is amplified by a signal amplifier and is subsequently sent to a real-time controller. A digital signal processor (DSP: iBIS DSP7101A) calculates the control input commands based on the measured output. The control commands output from DSP is delivered to a servo amplifier to drive the actuator (i.e., motor). In addition, the measured vibration signals are recorded by a data-collecting device (CATEC INC, Cat System). Because the vehicle vibration frequency to be suppressed is about 4 Hz in this study, a sampling frequency of the experimental system was set as about 3 kHz. Therefore, the sampling frequency has sufficient bandwidth for the target resonance to be controlled and realizes a fast control cycle.

5.2. Experimental results and discussion

Figure 9 shows the experimental results. The upper and lower graphs show the time responses of the vehicle body vibrations and the control inputs, respectively. The black line represents the response without any active vibration control. The green line represents the ideal response to be realized. The red line represents the experimental result obtained by the proposed method.

Figure 9 clearly demonstrates the high control performance achieved by the proposed active damping strategy. Compared to the open-loop response represented by the black line, the excellent transient characteristic is realized as indicated by the red line, making the controlled result close to the ideal target response. The vibration appearing after 2.0 s indicated by the black line is hardly suppressed, whereas that indicated by the red line is considerably attenuated.

According to the control input values near 2.0 s during the backlash traversal, we can see that the controller successfully switches from the backlash mode to the contact mode.

5.3. Comparison with the case without backlash compensation

For comparative investigations, only a H_2 controller that does not involve any backlash compensation is also implemented. Figure 10 shows the comparison result. The response in the case without backlash compensation is indicated by the blue line.

The blue line shows a large overshoot as well as residual vibrations between 2.0 s and 3.0 s. This poor performance is due to the absence of backlash compensation.

Meanwhile, the proposed method, represented by the red line, improves the performance by suppressing the overshoot and residual vibration amplitude. This result proves that the aim of our backlash compensation strategy is achieved by r_k^{BL} with the properly tuned value. Note that this key parameter was simultaneously auto-tuned

together with the contact mode H_2 controller. The proposed tuning approach reduces the burden of designers in terms of subjective tuning tasks.

Table 4 summarizes the quantitative comparison between the experimental results presented above. The 2-norm of the control error between the ideal response and each vibration response is shown. The notable point is that the smallest value is given by the proposed approach. The 2-norm by the proposed approach is reduced by 51.1688% and 74.4953% compared to “Without compensation for backlash” and “Without control”, respectively.

Table 4 Quantitative performance comparison based on 2-norm of the control error between the ideal response and each vibration response

Each control result	Proposed method	Without compensation for backlash	Without control (Open loop response)
Values of the 2-norm	0.1868	0.3826	0.7326

5.4. Robustness against plant variation

The robustness of the controller tuned by the proposed approach is verified in this section. For this purpose, a fluctuation of -50% was newly set for the length of the backlash of the actual test device. Through the application of the same controller as that used in the previous sections to this fluctuated device, the robustness against changes in the backlash can be validated.

Figure 11 shows the comparison between the proposed approach and the open-loop response under the fluctuation in the actual backlash. Despite the fluctuation, the high vibration suppression is retained as indicated by the red line.

Compared to the case without backlash compensation as shown in Fig. 12, the importance of addressing backlash is also observed. The reduced overshoot as well as the lower residual vibrations reflect the robustness of the backlash compensation. Even though the backlash is changed, the jerk can be observed independently of the

fluctuation. Therefore, it allows switching of the control modes, leading to robust backlash compensation.

Table 5 summarizes the 2-norm of each vibration response when the backlash is changed. The 2-norm by the proposed approach is reduced by 60.6790% and 77.5419% compared to “Without compensation for backlash” and “Without control”, respectively. These results quantitatively demonstrate the robust performance of the active vibration controller.

Table 5 2-norm of each experimental result with the fluctuation in the backlash

Each control result	Proposed method	Without compensation for backlash	Without control (Open loop response)
Values of the 2-norm	0.1475	0.3751	0.6568

The limitation of this study is that it is necessary to further verify the robustness of the controller tuned by the proposed approach. Severer changes should be considered under additional conditions of the drivetrain dynamics.

6. Conclusion

For a drivetrain mechanism with nonlinear backlash, this study proposed a norm-limited SPSA-based optimized active vibration controller. First, a basic experimental device reflecting a simplified drivetrain was demonstrated. The mechanism reproduces both the contact mode and the backlash mode. For the contact mode, a model-based H_2 controller was employed as the baseline damping strategy. For backlash compensation, a simple control mode switching algorithm was applied to the H_2 controller. This reduces the shock when the drivetrain is transferred from the backlash mode to the contact mode while allowing the backlash to be traversed rapidly. In our novel systematic design algorithm, the key controller parameters that influence the transient vibration attenuation and the compensation for backlash were comprehensively auto-tuned with reduced burden. This was realized on the basis of NLSPSA with high calculation efficiency and stability of the iterative tuning process. Finally, the controller tuned by the proposed approach was experimentally verified with the actual test device.

The experimental results demonstrated that the proposed damping strategy significantly improves the transient response. Moreover, the robustness of the controller against changes in the backlash was experimentally confirmed.

In the future, severer fluctuations will be tested for additional conditions of the drivetrain dynamics. In addition, a more robust controller will be developed by introducing an SPSA-based online tuning mechanism into the active damping strategy.

Declaration of competing interest

The authors declare that there is no conflict of interest.

Funding

The authors disclosed receipt of the following financial supports for the research, authorship, and/or publication of this article: This work was partly supported by the Transmission Research Association for Mobility Innovation (TRAMI) [23B3-01] and

the Japan Society for the Promotion of Science (JSPS) KAKENHI [Grant Number 22K20396; Grant Number 23K13273].

References

1. Raei M, Dardel M. Tuned mass damper and high static low dynamic stiffness isolator for vibration reduction of beam structure. *Proc Inst Mech Eng Part K J Multi-body Dyn* 2020; 234: 95–115.
2. Duc Phuc V, Tran V-T. Optimization design for multiple dynamic vibration absorbers on damped structures using equivalent linearization method. *Proc Inst Mech Eng Part K J Multi-body Dyn* 2022; 236: 41–50.
3. Yücesan A, Mugan A. Development and control of an active torsional vibration damper for vehicle powertrains. *Proc Inst Mech Eng Part K J Multi-body Dyn* 2021; 235: 452–464.
4. Barin F, Heidari Shirazi K, M. Sedighi H. Classification of transient vibration of passenger cars powertrain. *Proc Inst Mech Eng Part K J Multi-body Dyn* 2023; 237: 442–460.
5. Haris A, Motato E, Theodossiades S, et al. A study on torsional vibration attenuation in automotive drivetrains using absorbers with smooth and non-smooth nonlinearities. *Appl Math Model* 2017; 46: 674–690.
6. Ma K, Du J, Liu Y, et al. Torsional vibration attenuation of a closed-loop engine crankshaft system via the tuned mass damper and nonlinear energy sink under multiple operating conditions. *Mech Syst Signal Process* 2024; 207: 110941.
7. Vadamalu RS, Beidl C. Adaptive internal model-based harmonic control for active torsional vibration reduction. *IEEE Trans Ind Electron* 2020; 67: 3024–3032.
8. Chen X, Peng D, Hu J, et al. Adaptive torsional vibration active control for hybrid electric powertrains during start-up based on model prediction. *Proc Inst Mech Eng Part D J Automob Eng* 2021; 095440702110561.
9. Zhang X, Liu H, Zhan Z, et al. Modelling and active damping of engine torque ripple in a power-split hybrid electric vehicle. *Control Eng Pract* 2020; 104: 104634.
10. Liu H, Zhang X, Chen Y, et al. Active damping of driveline vibration in

power-split hybrid vehicles based on model reference control. *Control Eng Pract* 2019; 91: 104085.

11. Yue Y, Huang Y, Hao D, et al. Model reference adaptive LQT control for anti-jerk utilizing tire-road interaction characteristics. *Proc Inst Mech Eng Part D J Automob Eng* 2021; 235: 1670–1684.
12. Reddy P, Shahbakhti M, Ravichandran M, et al. Drivetrain clunk control via a reference governor. *IFAC-PapersOnLine* 2021; 54: 846–851.
13. Yonezawa H, Kajiwara I, Sato S, et al. Vibration control of automotive drive system with nonlinear gear backlash. *J Dyn Syst Meas Control Trans ASME* 2019; 141: 1–11.
14. Zhou Z, Guo R. A Disturbance-Observer-Based Feedforward-Feedback Control Strategy for Driveline Launch Oscillation of Hybrid Electric Vehicles Considering Nonlinear Backlash. *IEEE Trans Veh Technol* 2022; 71: 3727–3736.
15. Zhou Z, Guo R, Liu X. A disturbance-compensation-based sliding mode control scheme on mode switching condition for hybrid electric vehicles considering nonlinear backlash and stiffness. *J Vib Control* 2022; 107754632210961.
16. Lv C, Zhang J, Li Y, et al. Mode-switching-based active control of a powertrain system with non-linear backlash and flexibility for an electric vehicle during regenerative deceleration. *Proc Inst Mech Eng Part D J Automob Eng* 2015; 229: 1429–1442.
17. Zhang J, Chai B, Lu X. Active oscillation control of electric vehicles with two-speed transmission considering nonlinear backlash. *Proc Inst Mech Eng Part K J Multi-body Dyn* 2020; 234: 116–133.
18. Oglieve CJ, Mohammadpour M, Rahnejat H. Optimisation of the vehicle transmission and the gear-shifting strategy for the minimum fuel consumption and the minimum nitrogen oxide emissions. *Proc Inst Mech Eng Part D J Automob Eng* 2017; 231: 883–899.
19. Eckert JJ, Santiciolli FM, Silva LCA, et al. Vehicle drivetrain design multi-objective optimization. *Mech Mach Theory* 2021; 156: 104123.
20. Eckert JJ, da Silva SF, Santiciolli FM, et al. Multi-speed gearbox design and shifting control optimization to minimize fuel consumption, exhaust emissions

and drivetrain mechanical losses. *Mech Mach Theory* 2022; 169: 104644.

21. Eckert JJ, Barbosa TP, Silva FL, et al. Optimum fuzzy logic controller applied to a hybrid hydraulic vehicle to minimize fuel consumption and emissions. *Expert Syst Appl* 2022; 207: 117903.
22. McGehee J, Yoon H-S. Optimal torque control of an integrated starter–generator using genetic algorithms. *Proc Inst Mech Eng Part D J Automob Eng* 2015; 229: 875–884.
23. Mall P, Fidlin A, Krüger A, et al. Simulation based optimization of torsional vibration dampers in automotive powertrains. *Mech Mach Theory* 2017; 115: 244–266.
24. Ravichandran M, Doering J, Johri R, et al. Design and Evaluation of EV Drivetrain Clunk and Shuffle Management Control System. *Proc Am Control Conf* 2020; 2020-July: 4905–4912.
25. Lin C, Sun S, Walker P, et al. Off-line optimization based active control of torsional oscillation for electric vehicle drivetrain. *Appl Sci*; 7. Epub ahead of print 2017. DOI: 10.3390/app7121261.
26. Catenaro E, Formentin S, Corno M, et al. Auto-calibration with Stability Margins for Active Damping Control in Electric Drivelines. *2022 Eur Control Conf ECC 2022* 2022; 1186–1191.
27. Li A, Qin D. Adaptive model predictive control of dual clutch transmission shift based on dynamic friction coefficient estimation. *Mech Mach Theory* 2022; 173: 104804.
28. Rostiti C, Liu Y, Canova M, et al. A Backlash Compensator for Drivability Improvement Via Real-Time Model Predictive Control. *J Dyn Syst Meas Control Trans ASME*; 140. Epub ahead of print 2018. DOI: 10.1115/1.4039562.
29. Formentini A, Oliveri A, Marchesoni M, et al. A Switched Predictive Controller for an Electrical Powertrain System with Backlash. *IEEE Trans Power Electron* 2017; 32: 4036–4047.
30. Lu X, Lu T, Chai B. Mode-switch model predictive controller with “pre-contact” method for alleviating driveline vibration of electric vehicles considering backlash. *Proc Inst Mech Eng Part D J Automob Eng* 2020; 234: 2176–2194.

31. Atabay O, Ötkür M, Ereke İM. Model based predictive engine torque control for improved drivability. *Proc Inst Mech Eng Part D J Automob Eng* 2018; 232: 1654–1666.
32. Yonezawa H, Kajiwara I, Nishidome C, et al. Active vibration control of automobile drivetrain with backlash considering time-varying long control period. *Proc Inst Mech Eng Part D J Automob Eng* 2021; 235: 773–783.
33. Yonezawa H, Yonezawa A, Kajiwara I. Efficient Tuning Scheme of Mode-Switching-Based Powertrain Oscillation Controller Considering Nonlinear Backlash. *IEEE Access* 2023; 11: 93935–93947.
34. Yonezawa H, Yonezawa A, Hatano T, et al. Fuzzy-reasoning-based robust vibration controller for drivetrain mechanism with various control input updating timings. *Mech Mach Theory* 2022; 175: 104957.
35. Yonezawa H, Kajiwara I, Nishidome C, et al. Vibration control of automotive drive system with backlash considering control period constraint. *J Adv Mech Des Syst Manuf* 2019; 13: 1–16.
36. Gerdes JC, Kumar V. An impact model of mechanical backlash for control system analysis. In: *Proceedings of 1995 American Control Conference - ACC'95*. American Autom Control Council, pp. 3311–3315.
37. Nordin M, Galic' J, Gutman P-O. New models for backlash and gear play. *Int J Adapt Control Signal Process* 1997; 11: 49–63.
38. Chilali M, Gahinet P. H∞ design with pole placement constraints: An LMI approach. *IEEE Trans Automat Contr* 1996; 41: 358–367.
39. Zhou K, Doyle JC, Glover K. *Robust and Optimal Control*. New Jersey: PrenticeHall, 1996.
40. Spall JC. Multivariate Stochastic Approximation Using a Simultaneous Perturbation Gradient Approximation. *IEEE Trans Automat Contr* 1992; 37: 332–341.
41. Spall JC. Implementation of the simultaneous perturbation algorithm for stochastic optimization. *IEEE Trans Aerosp Electron Syst* 1998; 34: 817–823.
42. Spall JC. An Overview of the Simultaneous Perturbation Method for Efficient Optimization. *Johns Hopkins Apl Tech Dig* 1998; 19: 482–492.

43. Spall JC. *Introduction to Stochastic Search and Optimization: Estimation, Simulation, and Control*. Hoboken, NJ, USA: John Wiley & Sons, Inc. Epub ahead of print 26 March 2003. DOI: 10.1002/0471722138.
44. Yonezawa A, Yonezawa H, Kajiwara I. Parameter tuning technique for a model-free vibration control system based on a virtual controlled object. *Mech Syst Signal Process* 2022; 165: 108313.
45. Tanaka Y, Azuma SI, Sugie T. Simultaneous perturbation stochastic approximation with norm-limited update vector. *Asian J Control* 2015; 17: 2083–2090.

Appendix

Nomenclature	
A	Positive constant with respect to a_k to perform SPSA
$\boldsymbol{A}_{ck}$	System matrix of state equation of H_2 controller at kth iteration
$\boldsymbol{A}_p$	State matrix of state equation of plant
a	Hyperparameter with respect to a_k to perform SPSA
a_k	Gain sequence required in SPSA at kth iteration
$\boldsymbol{B}_{ck}$	System matrix of state equation of H_2 controller at kth iteration
$\boldsymbol{B}_{p1}$	Disturbance matrix of state equation of plant
$\boldsymbol{B}_{p2}$	Input matrix of state equation of plant
bl	Dead zone width
c	Hyperparameter with respect to c_k to perform SPSA
C_C	Damper connected with M_B
$\boldsymbol{C}_{ck}$	System matrix of state equation of H_2 controller at kth iteration
C_D	Damper between M_B and m_G
C_G	Damper between M_E and m_G
C_{cl}	Damper of M_E
c_k	Gain sequence required in SPSA at kth iteration
$\boldsymbol{C}_p$	Output matrix of state equation of plant
C_{stop}	Stop criterion for optimization
d	Scalar-valued constant (upper bound of update vector) required in SPSA with norm-limited update vector
D_{ck}	System matrix of state equation of H_2 controller at kth iteration
$\boldsymbol{D}_{p1}$	Direct transmission matrix for $\boldsymbol{w}_p$ of state equation of plant
D_{p2}	Direct transmission matrix for u of state equation of plant
$e(n)$	Control error for $r(n)$
$e_{BL}(n)$	Control error for r_k^{BL}
F	Force originating from K_G

$F_{Highpass}$	Frequency weighting transfer function based on high-pass filter
$F_{Lowpass}$	Frequency weighting transfer function based on low-pass filter
$G(s)$	Expanded controlled object in H_2 controller design
$g(\theta)$	Gradient of $L(\theta)$ with respect to θ
$\hat{g}_k(\theta_k)$	Estimation of gradient vector $g(\theta)$ at kth iteration
$\hat{g}_{k,i}$	ith element of $\hat{g}_k$
$J(\theta_k)$	Loss function defined in this study
$Jerk(n)$	Jerk of vehicle body
k	Number of iterations for optimization
K_C	Spring connected with M_B
K_D	Spring between M_B and m_G
K_G	Spring between M_E and m_G
$L(\theta)$	Non-negative scalar loss function to be minimized by SPSA
M_B	Mass of vehicle body in simplified drivetrain
M_E	Mass of actuator in simplified drivetrain
m_G	Mass of intermediate part in simplified drivetrain
N	Number of total sampling points
n	Number of sampling step
OKG	Constant term of spring force in backlash model
p	Dimension of θ_k
P_c	Transfer function of controlled object in H_2 controller design
Q_k	Weighting constant in H_2 controller design at kth iteration
$r(n)$	Target response to be followed
R_k	Weighting constant in H_2 controller design at kth iteration
r_k^{BL}	Compensation reference signal in backlash mode control at kth iteration
Sw	Switching parameter to express dead-zone effect due to backlash
$T_{zw}(s)$	Transfer function from external input to z for $G(s)$
$Threshold$	Threshold value on vehicle jerk to switch control modes
u	Control input
$u_{BL}(n)$	Control input in backlash mode

$u_{CO}(n)$	Control input in contact mode
u_G	Control input from $G(s)$
$u_{k,n}$	Control input component at kth iteration at nth sampling step
w	Disturbance defined in H_2 controller design
$\boldsymbol{w}_p$	Disturbance including force due to backlash
W_y	Scaling factor on $\tilde{y}_{k,n}$ in loss function
W_u	Scaling factor on $u_{k,n}$ in loss function
$\boldsymbol{x}_{AW}(n)$	State vector of H_2 controller during anti-windup
X_B	Vibration response of M_B
$\boldsymbol{x}_c(n)$	State vector of H_2 controller
X_E	Vibration response of M_E
x_G	Vibration response of m_G
$\boldsymbol{x}_p$	State vector of plant
y	Measured output defined in H_2 controller design
y_G	Vehicle vibration from $G(s)$
y_p	Measured output (Vehicle body vibration) from plant
$\tilde{y}_{k,n}$	Control error at kth iteration at nth sampling step
z	Controlled variable vector
z^{-1}	One-cycle delay operator
z_y	Controlled variable for transient response in H_2 controller design
z_u	Controlled variable for penalty on control input amount in H_2 controller design
α	Positive constant with respect to a_k to perform SPSA
γ	Positive constant with respect to c_k to perform SPSA
δ	Saturation function
Δ_k	Random perturbation vector with Bernoulli distribution
$\Delta_{k,i}$	ith element of Δ_k
θ	Design variable

θ_k	Design variable updated by SPSA at kth iteration
$\theta_{k,i}$	ith component of θ_k

Abbreviations

Abbreviation	Description
GA	Genetic algorithm
LQR	Linear quadratic regulator
MPC	Model predictive control
NLSPSA	Norm-limited update vector-based simultaneous perturbation stochastic approximation
PD baseline controller	Proportional-derivative baseline controller
PID controller	Proportional integral differential controller
RMS	Root mean square
SPSA	Simultaneous perturbation stochastic approximation

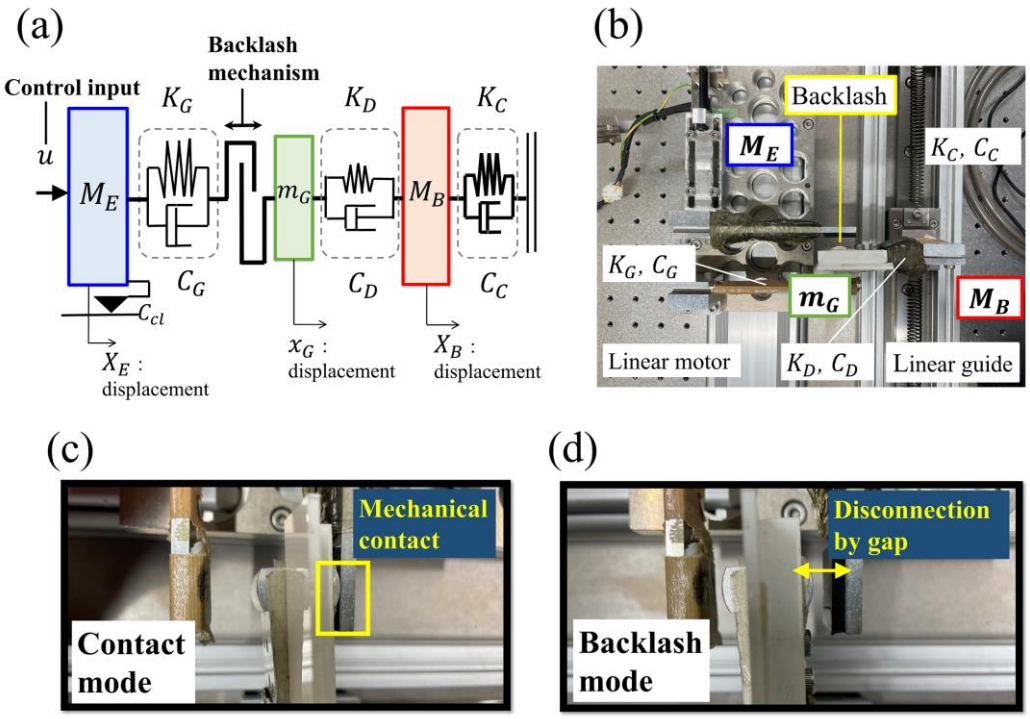

Fig. 1. Basic experimental device: (a) drivetrain model; (b) real test device; (c) contact mode; (d) backlash mode.

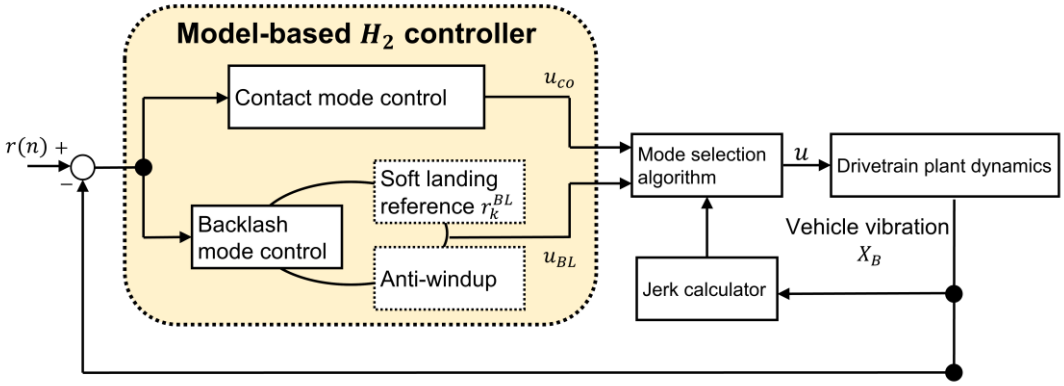

Fig. 2. Active damping strategy composed of backlash and contact mode controls.

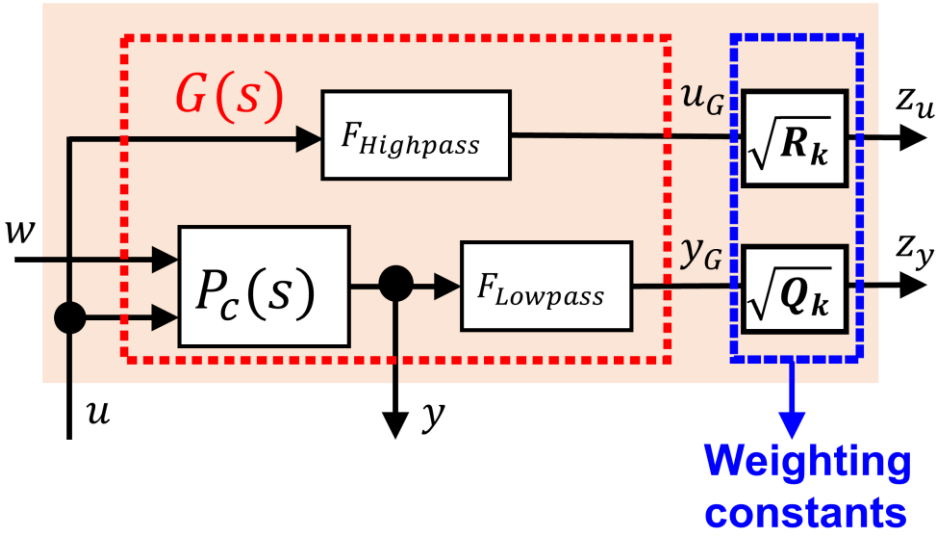

Fig. 3. Generalized plant used to design the contact mode controller.

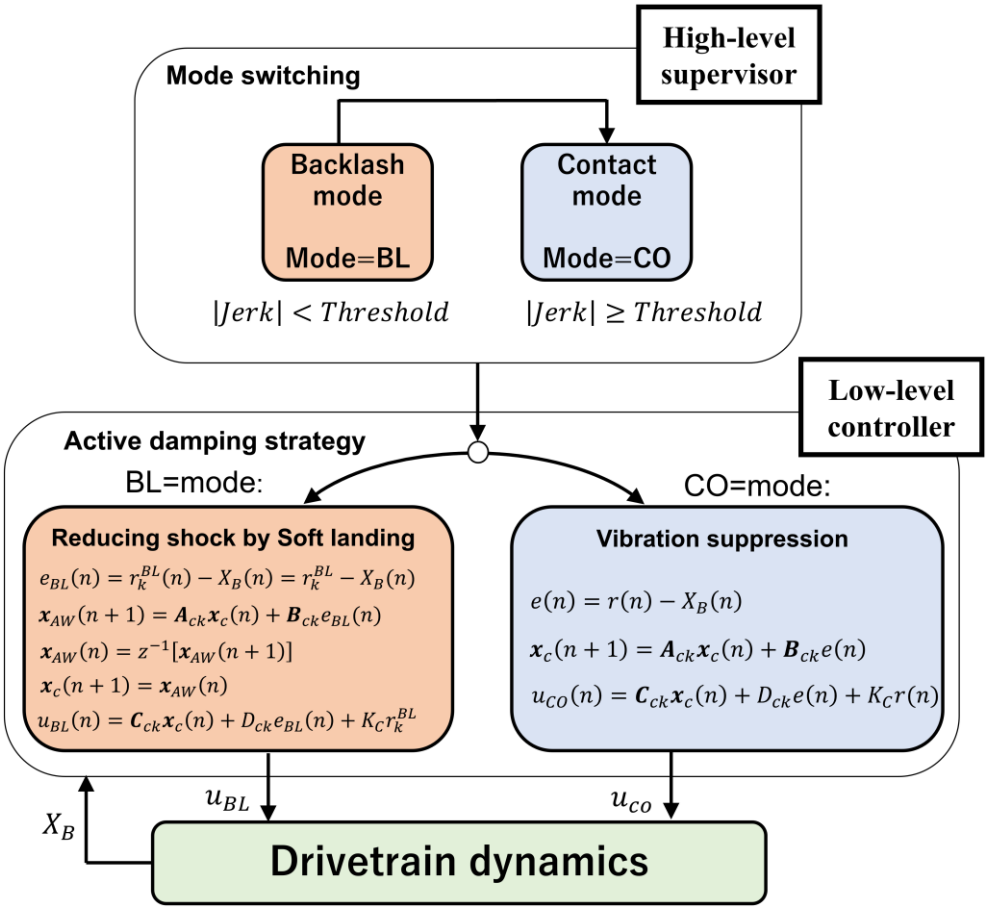

Fig. 4. Simple control mode switching algorithm.

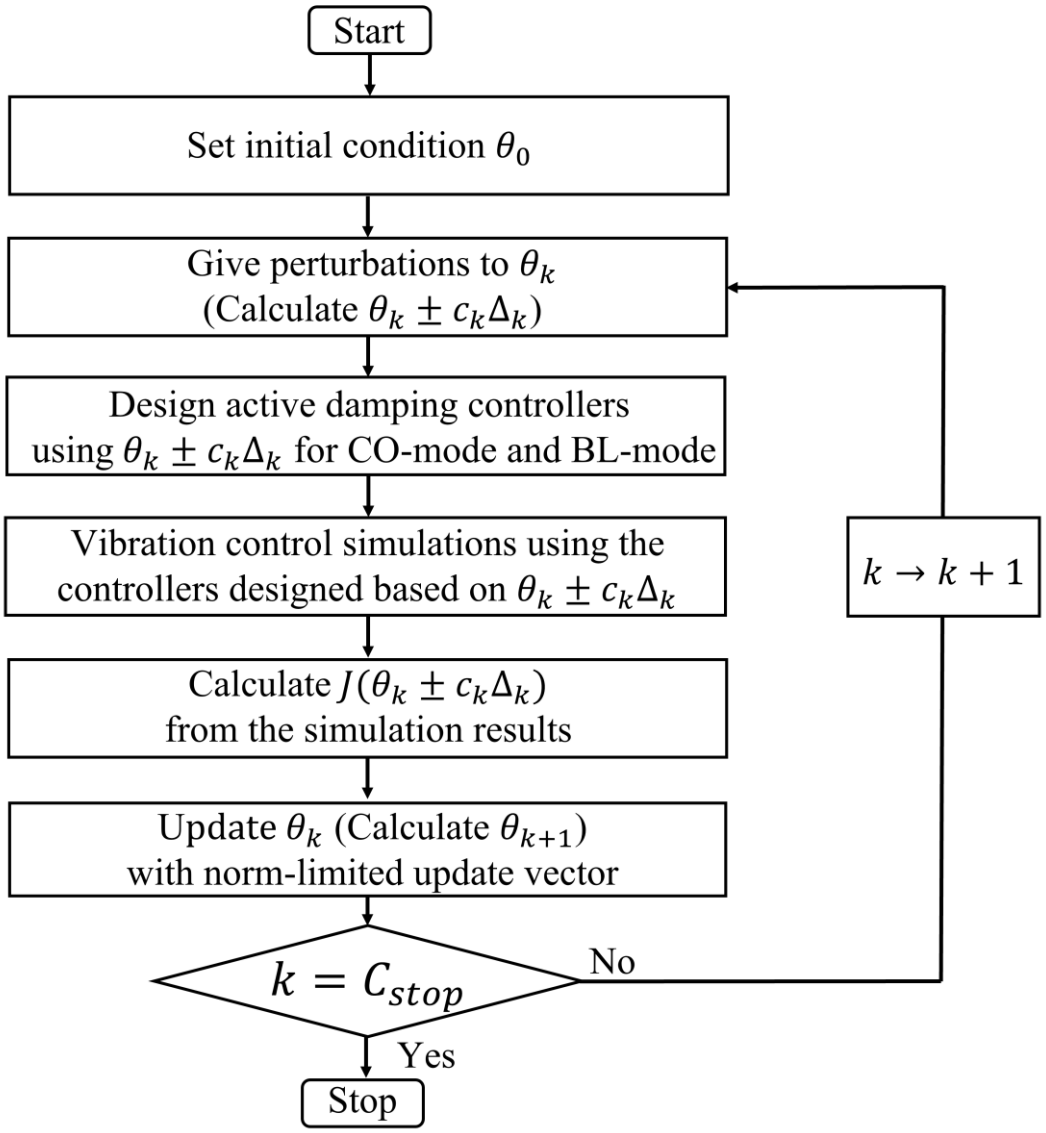

Fig. 5. Tuning scheme for the controller design parameters using SPSA with norm-limited update vector.

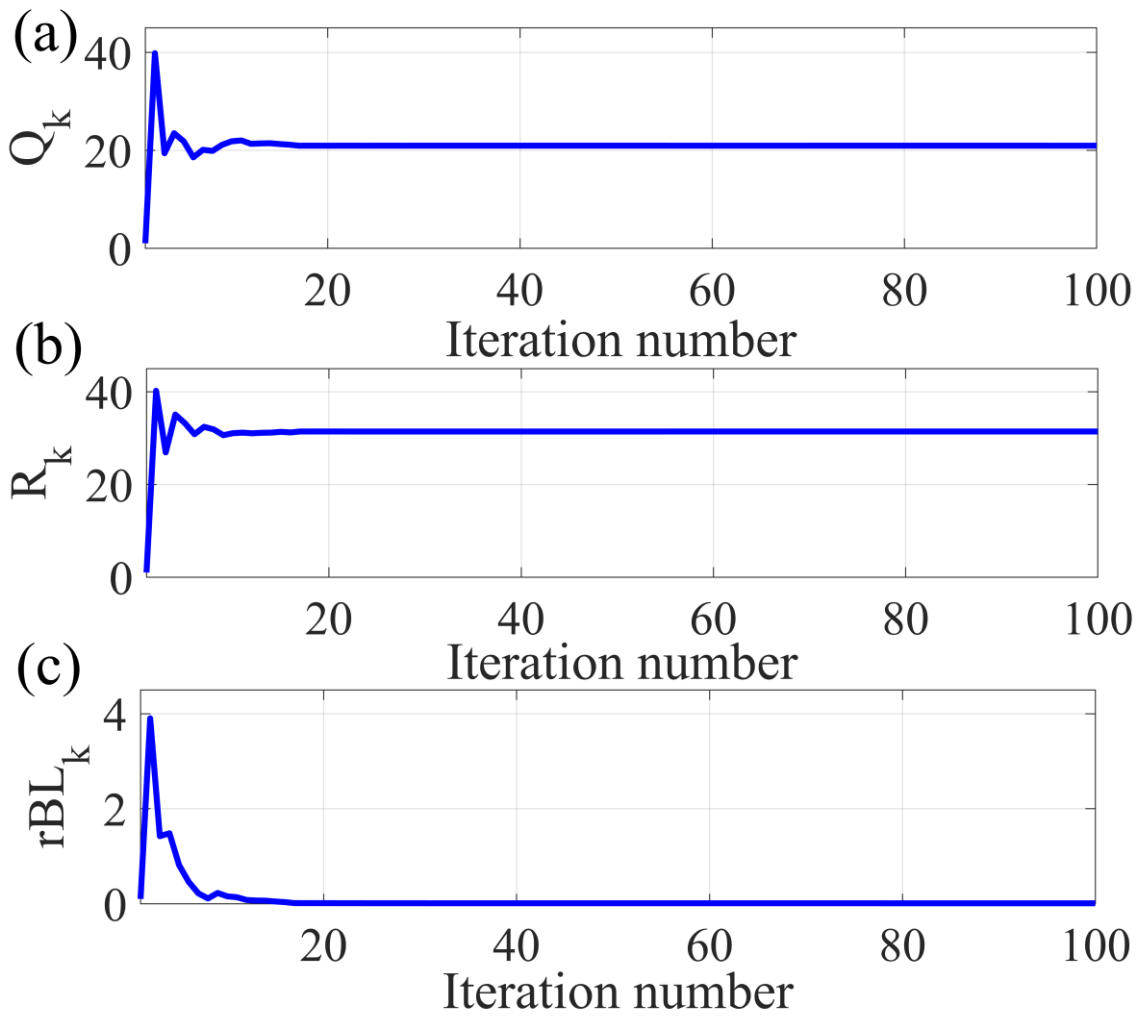

Fig. 6. Tuning history of each tuning parameter: (a) Q_k; (b) R_k; (c) r_k^{BL}.

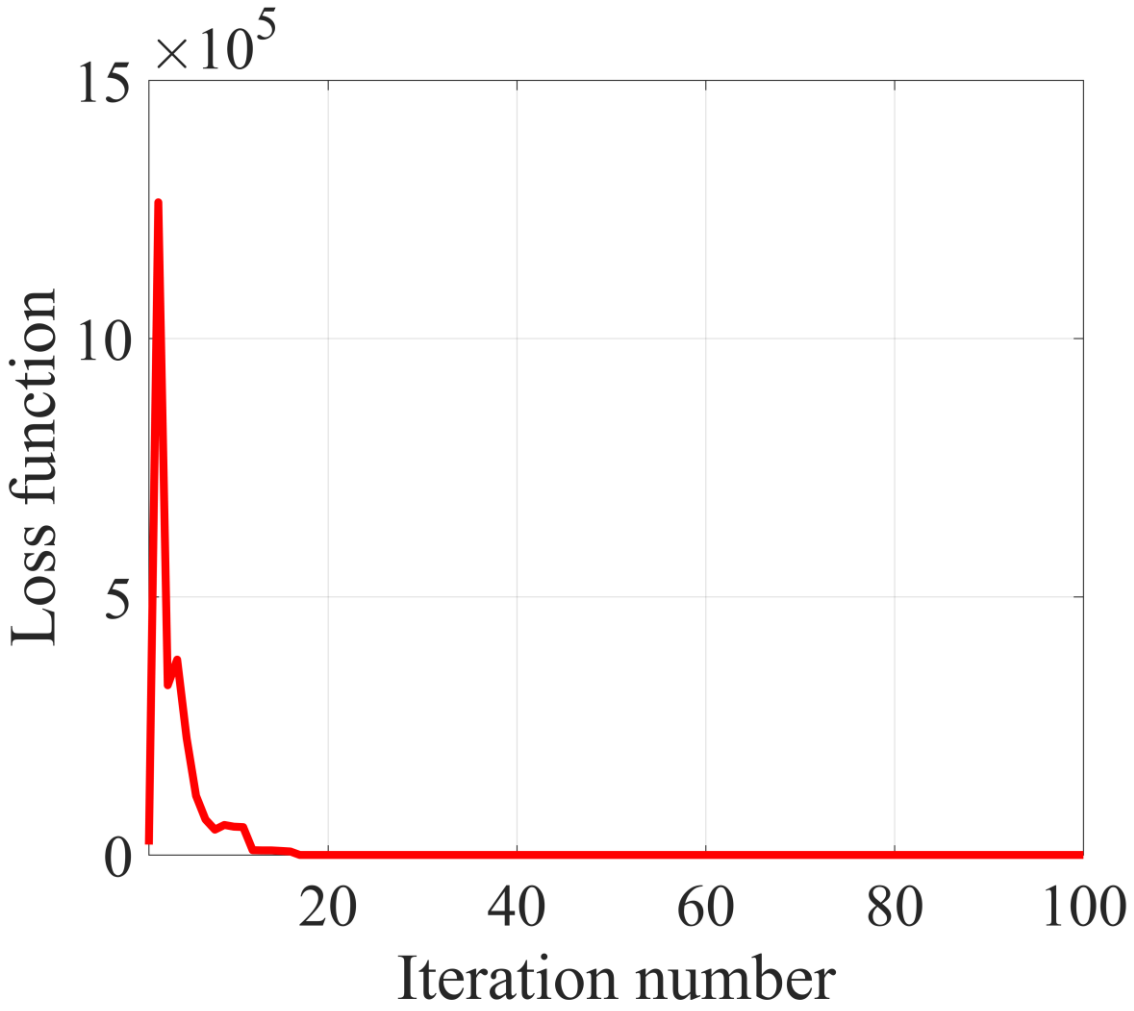

Fig. 7. Tuning history of the loss function.

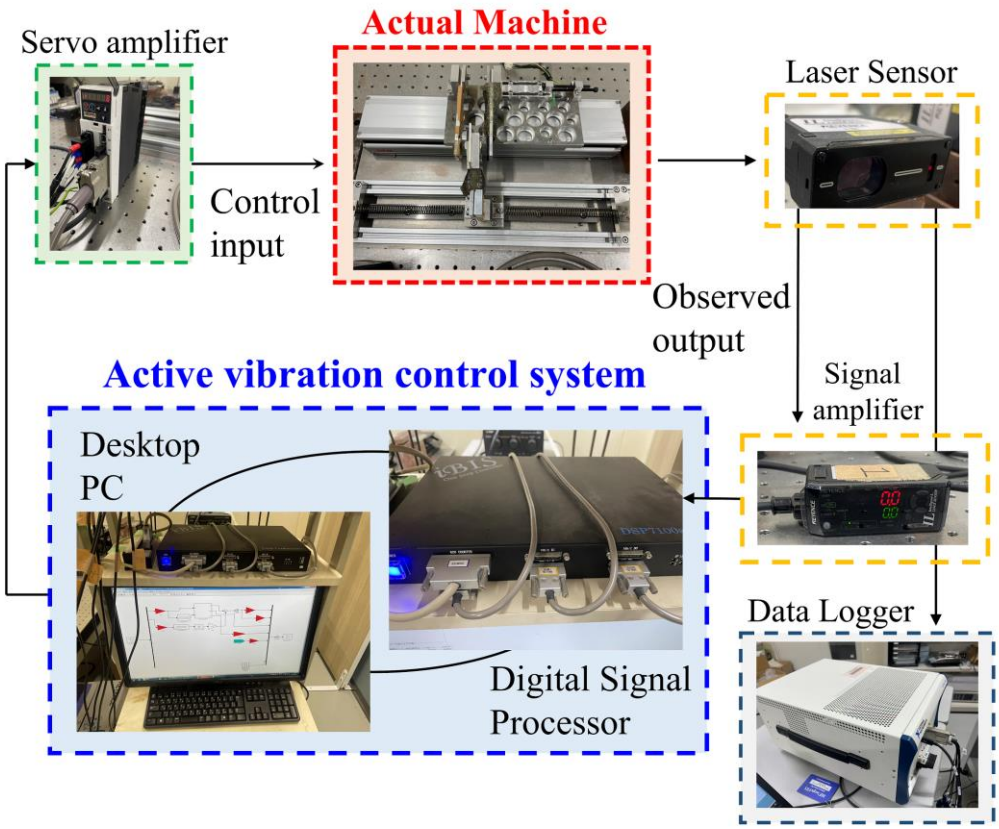

Fig. 8. Closed-loop diagram of the experimental system.

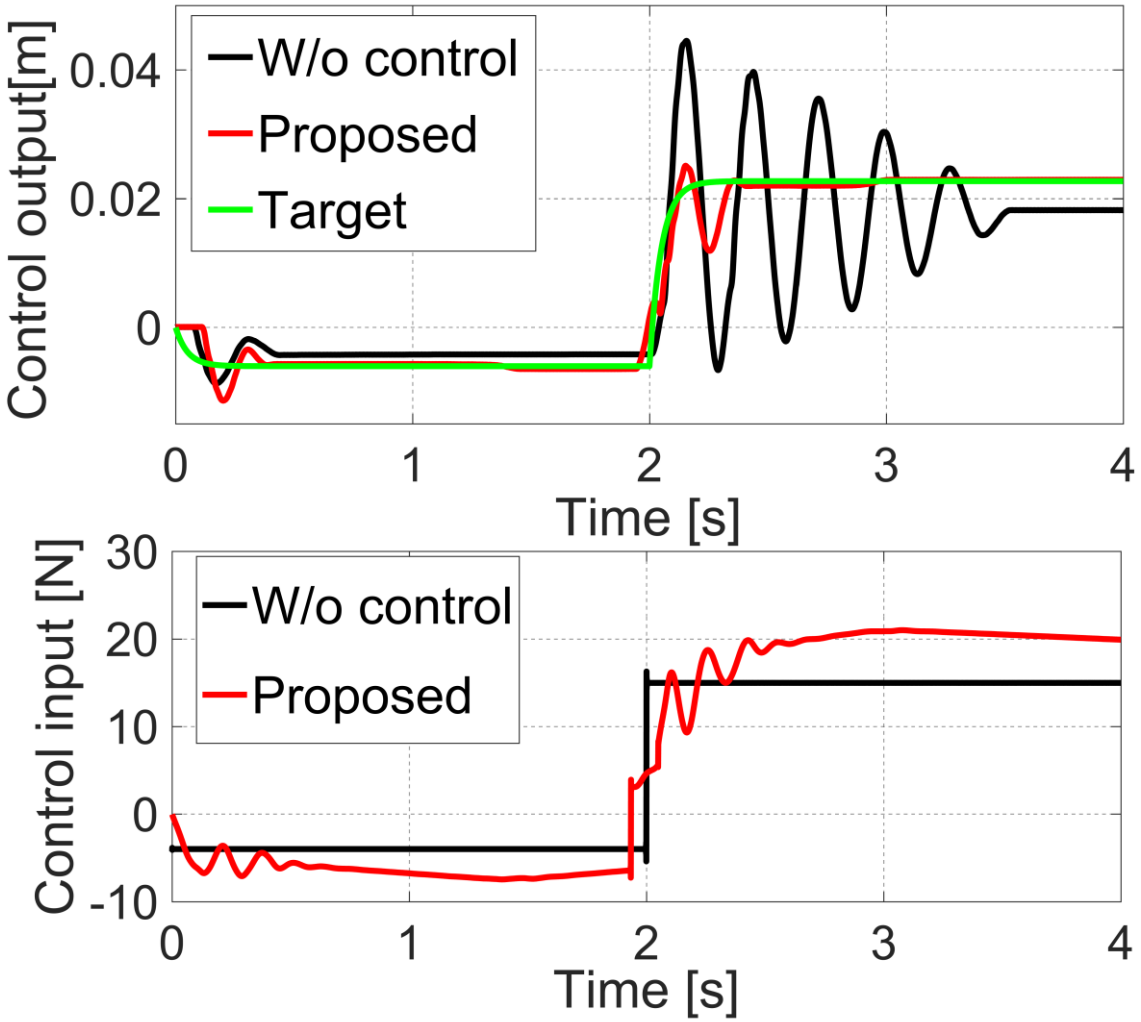

Fig. 9. Vehicle body vibration response and control input measured by the experimental verification.

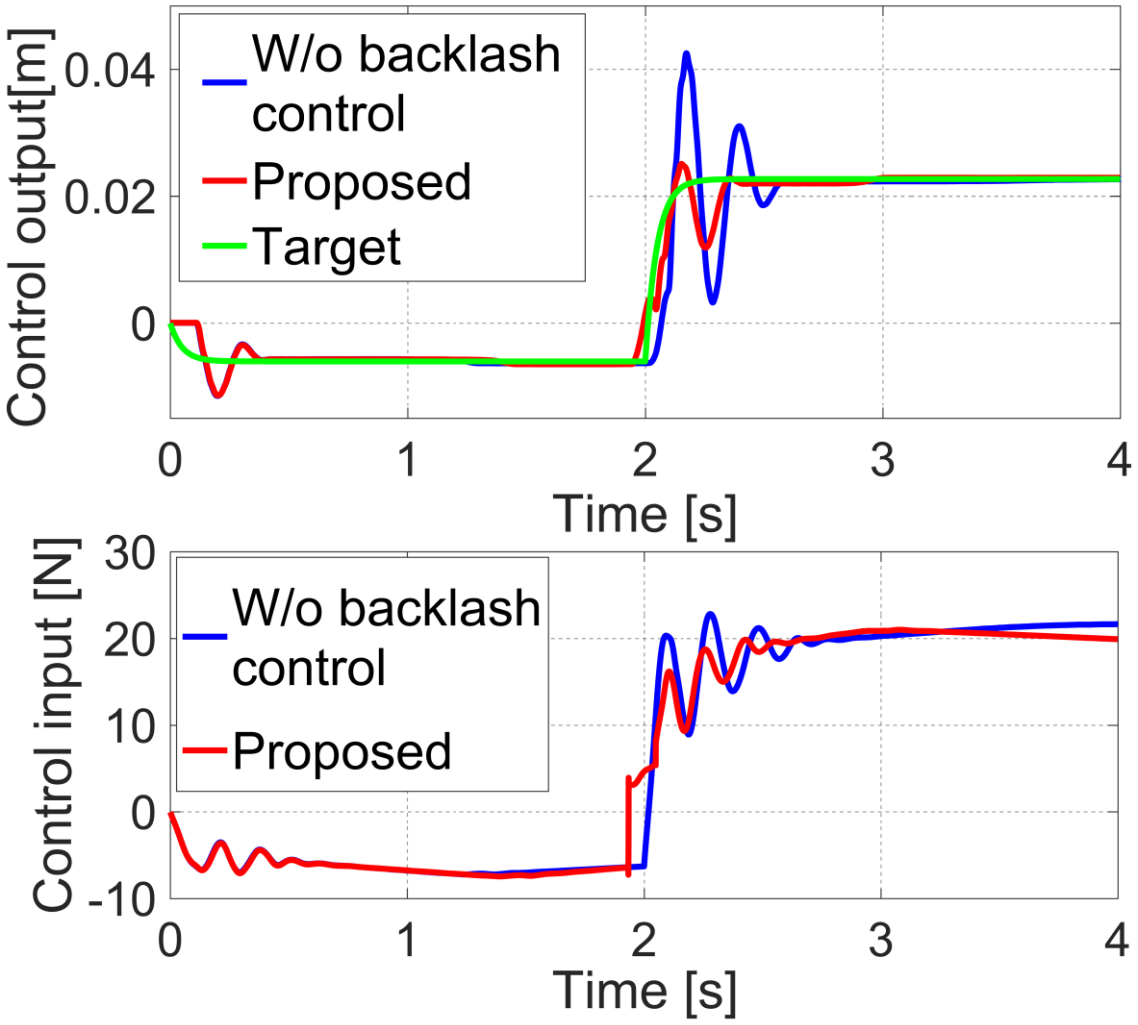

Fig. 10. Comparison between the proposed approach and case without compensation for backlash.

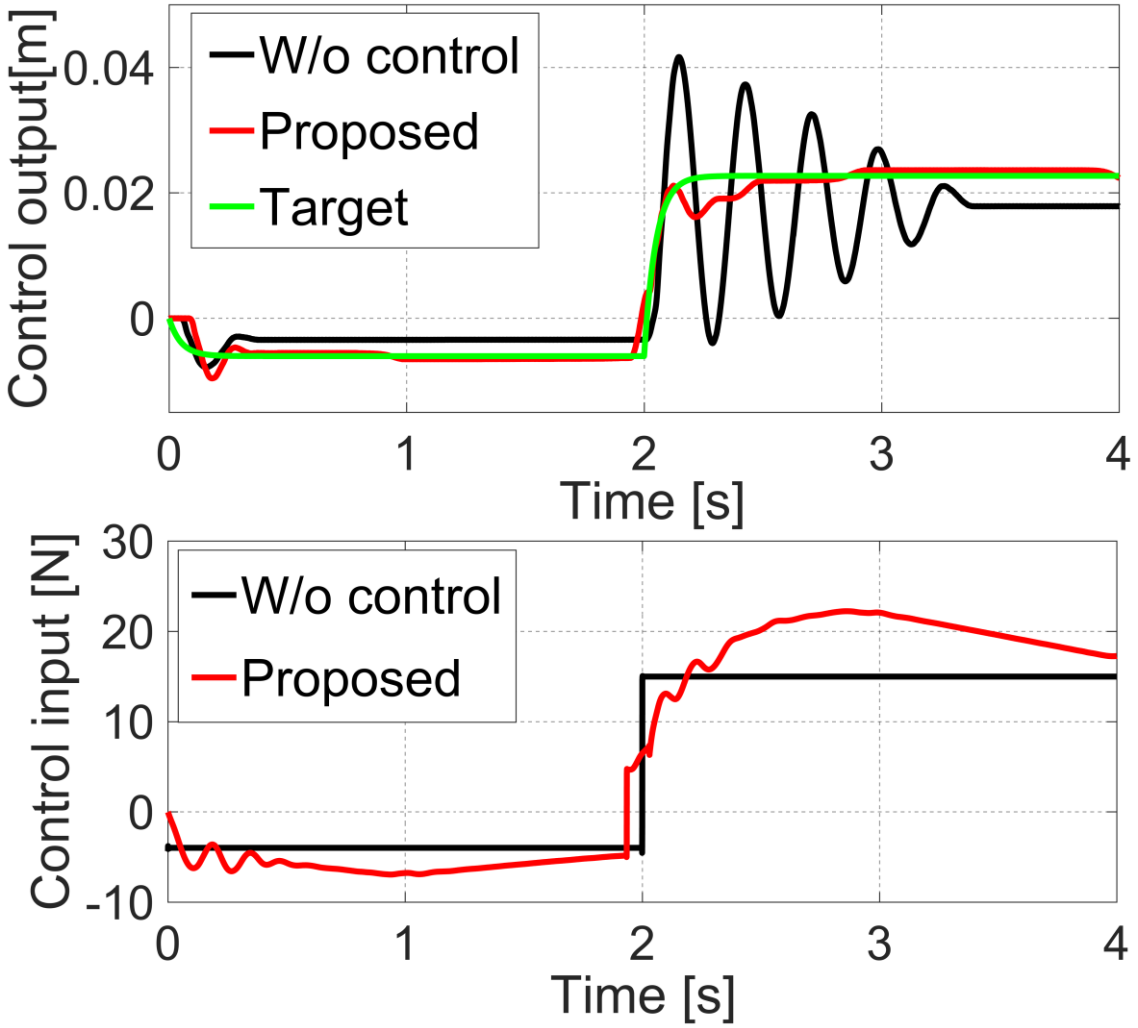

Fig. 11. Vehicle body vibration response and control input with the fluctuation of the backlash.

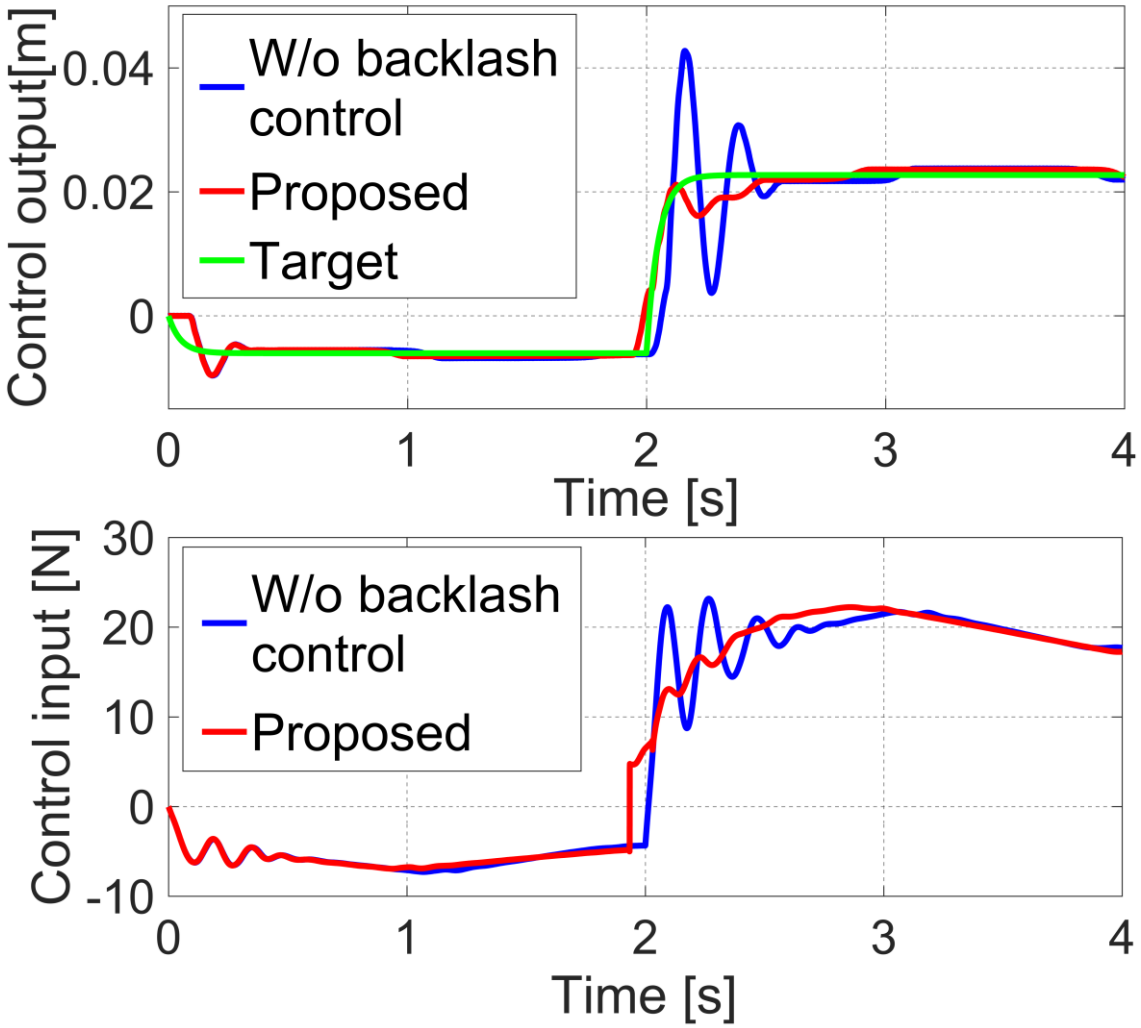

Fig. 12. Comparison between the proposed approach and the case without backlash compensation when there is a fluctuation in the backlash.